'In situ' formation and voltammetric characterization of polymeric linear [(Mn(H2O)3)2(H2W12O42)]n6n- polyoxometalates in vertically-oriented mesoporous silica thin films

Neus Vilà, Clara Richart, David Nieto, Mariela Brites-Helu, Israël Mbomekallé, Alain Walcarius

‘In situ’ formation and voltammetric characterization of polymeric linear $[(Mn(H_2O)_3)_2(H_2W_{12}O_{42})]_n^{6n-}$ polyoxometalates in vertically-oriented mesoporous silica thin films

Neus Vilà,[a,*] Clara Richart,[a] David Nieto,[b] Mariela Brites-Helu,[a] Israël Mbomekallé[b*] and Alain Walcarius[a]

[a] *Université de Lorraine, CNRS, LCPME, F-54000 Nancy, France*

[b] *Université Paris Saclay, CNRS, ICP, F-91405 Orsay, France*

* *Corresponding author: neus.vila@univ-lorraine.fr; israel.mbomekalle@universite-paris-saclay.fr*

Abstract

We present in this paper the ‘in situ’ preparation of manganese-containing polyoxotungstate $[Mn(H_2O)_3)_2(H_2W_{12}O_{42})]_n^{6n-}$ (**1**) chains in vertically-oriented mesoporous silica thin films on indium-tin oxide (ITO) electrodes. Taking advantage of a soft sequential method allowing the formation of **1** inside the mesoporous matrix, we succeed in its ‘in situ’ formation according to two main steps: (i) a first one consisting of the immobilization of $[Mn(H_2O)_6]^{2+}$ in sulfonate-functionalized silica thin films; and (ii) a second one involving the reaction of the $[Mn(H_2O)_6]^{2+}$ moieties with $Na_2WO_4{\bullet}2H_2O$. The electrochemical characterization of the functionalized materials obtained clearly demonstrates that the content of sulfonate groups in the starting films is a critical parameter to get the expected electroactive $[Mn(H_2O)_3)_2(H_2W_{12}O_{42})]_n^{6n-}$ compound inside the silica nanochannels. The experimentally determined chemical composition of the films performed by X-ray Photoelectron spectroscopy (XPS) is in good agreement with the expected composition of **1** in the case of films obtained with the optimal content of sulfonate

functions (*i.e.*, 5-6.5% sulfonate with respect to silica). Energy Dispersive analysis of X-rays coupled with Transmission Electron Microscopy (TEM-EDX) carried out on the cross section of the films show that a uniform composition in terms of Mn/W ratio is obtained after the functionalization process. This confirms the formation of $[Mn(H_2O)_3)_2(H_2W_{12}O_{42})]_n^{6n-}$ uniformly within the whole thickness of the silica film (*i.e.*, 80 nm), explaining also the long-range charge transfer reactions occurring through such insulating silica membrane. Using sulfonated silica films as template, we develop a robust 'in situ' synthesis strategy to assemble 1D linear polyoxotungstates onto ITO electrodes, exhibiting a stable electrochemical response once confined within the silica nanochannels.

Keywords: 1D linear polyoxotungstates, vertically-oriented mesoporous silica films, modified electrode, long-range charge transport.

1. Introduction

Nanoporous solids have a large surface area, nanosized walls, and three-dimensionally porous networks, making them potential candidates for gas adsorption, separation, and heterogeneous catalysis [1, 2]. In this regard, the ordered mesoporous silicates are of particular interest due to the possibility of preparing materials exhibiting well-controlled nanostructures with tunable porosity and functionality [3]. They can be also manufactured in the form of thin membranes with preferential pore orientation [4-7]. The confinement of molecular chains in an oriented template can lead to unique and improved electronic, electrochemical, optical or mechanical properties of the nanocomposites thus obtained (*e.g.*, as reported for conducting polymers [8, 9]). A controlled spatial arrangement (*i.e.*, regular distribution at the nanoscale) might also be of interest to promote efficient charge transfer processes, with particular interest for nanoreactors and sensors [10,11].

Polyoxometalates (POMs) are inorganic anionic compounds that consist of metal oxo clusters. These clusters are often composed of early transition metals, such as tungsten or molybdenum in their highest oxidation state, surrounded by oxygen atoms and containing heteroatoms with nanosized geometry. They exhibit rich electrochemical behaviour without significant changes in their structure [12-15], making them promising candidates for applications in electrocatalysis, energy conversion or electrochemical sensing [15-19]. However, for practical uses, POMs often need to be confined onto electrode surfaces. This can be achieved in particular via chemisorption, electrodeposition, encapsulation in polymers or inorganic matrices, and deposition as monolayers (Langmuir-Blodgett process) or multilayers (layer-by-layer assembly) [17, 19-24]. The use of POMs in the design and synthesis of hybrid materials or functional nanostructures is attractive due to their unique features such as high negative charge density, redox activity, available organic grafting and unique ligand properties [25, 26]. The use of supramolecular assemblies as templates, however, implies that these larger structures could guide the formation and assembly of other organized molecular assemblies [27]. Incorporating POMs into such mesoporous hosts may provide several advantages for practical applications by preventing their dissolution or aggregation for instance.

Here we provide a simple method to confine 'in situ' a manganese-containing polyoxotungstate ($[Mn(H_2O)_3)_2(H_2W_{12}O_{42})]_n^{6n-}$) in vertically-oriented mesoporous silica thin films while retaining its intrinsic electrochemical activity. This first involves the electro-assisted generation of sulfonate functionalized mesoporous silica films on ITO electrodes, followed by their reaction with $[Mn(H_2O)_6]^{2+}$ and then with $Na_2WO_4 \bullet 2H_2O$. The resulting hybrid films are electroactive and their electrochemical response depends on the amount of sulfonate groups in the starting material, a critical parameter affecting the formation of $[Mn(H_2O)_3)_2(H_2W_{12}O_{42})]_n^{6n-}$ in the nanochannels, as supported by TEM-EDX and XPS characterization.

2. Experimental section

2.1. Chemicals and reagents

Tetraethoxysilane (TEOS, 98%, Alfa Aesar), 3-mercaptopropyltrimethoxysilane (MPTMS, 95%, sigma Aldrich), ethanol (95-96%, Merck), sodium nitrate ($NaNO_3$, 98%, Prolabo), sodium tungstate dihydrate ($Na_2WO_4 \bullet 2H_2O$, ≥99%, Sigma-Aldrich), manganese acetate tetrahydrate ($Mn(CH_3COO)_2 \bullet 4H_2O$, >99%, Sigma-Aldrich), zinc acetate dihydrate ($Zn(CH_3COO)_2 \bullet 2H_2O$, Sigma Aldrich), potassium chloride (KCl, >99%, Sigma-Aldrich), hydrochloric acid (HCl, 36.5-38% Riedel de Haen), sulfuric acid (H_2SO_4, 98%, Sigma-Aldrich), cetyltrimethylammonium bromide (CTAB, 99%, Acros) and octadecyltrimethylammonium bromide (ODAB) have been used as received. $[(Mn(H_2O)_3)_2H_2W_{12}O_{42}]_n^{6n-}$ (actually its powdered form $K_2Na_4[(Mn(H_2O)_3)_2H_2W_{12}O_{42}] \bullet 28H_2O$) was prepared by following a synthetic procedure previously reported [28].

2.2. Preparation of sulfonate-functionalized vertically-aligned mesoporous silica films

The preparation of sulfonate-functionalized vertically-oriented silica thin films on ITO plates (surface resistivity 8−12 Ω, Delta Technologies) was carried out as previously described [29]. The first step consists of the preparation of thiol-modified silica thin films by the EASA procedure adapted from [30]. A hydroalcoholic solution (20 mL H_2O + 20 mL EtOH) containing 100 mM of the silica precursors (TEOS and MPTMS), 32 mM of surfactant template (CTAB or ODAB) and 0.1 M of supporting electrolyte ($NaNO_3$), was prepared and its pH was adjusted to 3 by adding 0.1 M HCl. The ratio MPTMS/TEOS varied from 2.5/97.5 to 8/92. After a first step of sol aging for 2.5 h to ensure proper hydrolysis of the precursors, a cathodic potential of -1.3 V was applied for 20 s to the ITO working electrode to initiate the oriented growth of the thiol-functionalized mesoporous silica layer. The film electrode was thoroughly

rinsed with water and aged overnight at 130°C. Extraction of the surfactant template was achieved by immersing the film electrode in an ethanol solution containing 0.1 M HCl for 15 min. The thiol groups in the films were then chemically oxidized into sulfonate groups (see top left of Scheme 1) by using hydrogen peroxide as previously described [29].

2.3. 'In situ' formation of $[(Mn(H_2O)_3)_2(H_2W_{12}O_{42})]_n^{6n-}$ in the oriented silica channels

The 'in situ' synthesis of $[(Mn(H_2O)_3)_2(H_2W_{12}O_{42})]_n^{6n-}$ in vertically-oriented sulfonate-functionalized silica thin films was performed by adapting the synthetic protocol applied to form the corresponding powder [28] to the particular case of the silica films given their chemical stability. A first step of the synthesis consists of the impregnation of sulfonate-functionalized films in a solution 10 mM manganese (II) acetate tetrahydrate for 1h (see top right of Scheme 1). Subsequently, the manganese-containing films ($[Mn(H_2O)_6]^{2+}SO_3^-@SiO_2$) were thoroughly rinsed with ethanol. A solution of 3.0 g sample of $Na_2WO_4 \bullet 2H_2O$ (9.1 mmol) dissolved in 5 mL of water was slowly added upon stirring at room temperature to a 0.11 g sample of $Zn(CH_3COO)_2 \bullet 2H_2O$ (0.5 mmol) dissolved in 18 mL of acetate buffer (0.5 M CH_3COONa + 0.5 M CH_3COOH). The pH of this solution is close to 8 after completing the addition of $Na_2WO_4 \bullet 2H_2O$ and is adjusted to 6 by addition of 1 M CH_3COOH to keep the medium compatible with the chemical stability of silica. The cloudy solution obtained was heated at 50°C for about 15 min. The manganese-containing films primarily prepared were dipped in this solution at 65°C for 1h to generate the manganese-containing polyoxotungstate chains inside the vertical nanochannels (see bottom of Scheme 1). The films were subsequently rinsed with the acetate buffer solution and dipped in a 1 M KCl solution for 5 min in order to remove any residual reaction products (such as highly soluble isopolytungstate or tungstate-based salts). They are denoted $[Mn_2W_{12}O_{42}]POM\text{-}SO_3^-@SiO_2$.

2.4. Apparatus

Film syntheses and electrochemical characterizations were carried out using an µAutolab potentiostat driven by the NOVA software (Methrom, France). A home-made one-compartment electrochemical cell with a classical three-electrode configuration was used for film synthesis (see supplementary material in Ref. [31]). A one-compartment cell with a standard three-electrode configuration was used for cyclic voltammetry experiments. The reference electrode was a Ag/AgCl electrode separated from the bulk electrolyte solution via fritted compartments filled with the same electrolyte. The counter electrode was a stainless steel of large surface area (chemically stable in the conditions used here). The working electrode was an ITO plate coated, or not, with a mesoporous silica film, analysed over a disk area of 0.20 cm^2. Cyclic voltammograms have been recorded at scan rates varying from 10 mV s^{-1} to 100 mV s^{-1} from aqueous solutions of the POM at selected pH values and ionic strengths adjusted using H_2SO_4 and/or Na_2SO_4.

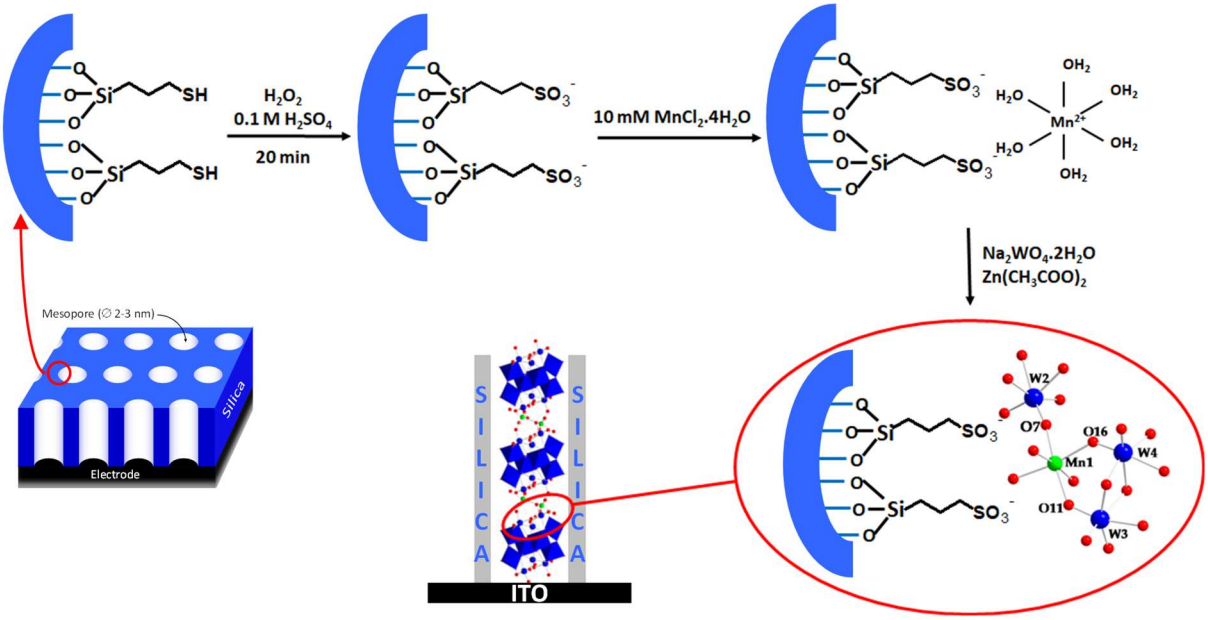

Scheme 1. Illustration of the procedure applied to immobilize $[Mn(H_2O)_3)_2(H_2W_{12}O_{42})]_n^{6n-}$ (**1**) on ITO electrode covered with an oriented sulfonate-functionalized mesoporous silica film.

3. Results and Discussion

The synthesis of $[(Mn(H_2O)_3)_2(H_2W_{12}O_{42})]^{6-}$ (**1, see** Figure S1 in Supporting Information) has been successfully achieved as described [28]. Single crystal X-ray analyses revealed a 2-D network structure. In the solid state, this manganese-containing polyoxotungstate forms linear chains of $[(Mn(H_2O)_3)_2(H_2W_{12}O_{42})]_n^{6n-}$, where $[H_2W_{12}O_{42}]^{10-}$ fragments are linked in pairs via Mn^{2+} ions. Detailed electrochemical studies have been carried out previously [28] using glassy carbon electrodes in aqueous solutions (pH range 1–6) where **1** is stable. $[Mn(H_2O)_3)_2(H_2W_{12}O_{42})]_n^{6n-}$ undergoes multiple electron-transfer processes that lead to the electrogeneration of high oxidation state manganese species that catalyse water electro-oxidation on the anodic side, and to the electroreduction of tungsten centres on the cathodic domain, which are also effective in the electrocatalytic reduction of nitrite or dioxygen. In this sense, the immobilization of such linear structures on electrode surfaces can offer several advantages for practical applications, helping to improve the stability of the POM by preventing leaching or aggregation. This can make it possible to obtain a more durable catalyst, reusable over multiple cycles. Depending on the immobilization method or the template employed for immobilization, one could control the orientation of the linear structures, which could influence the accessibility of active sites and improve catalytic efficiency. With this in mind, it appears that vertically-oriented mesoporous silica films (MSF) obtained by electrochemically-induced self-assembly (EASA [4, 7, 32]) could be ideal templates for immobilizing such linear $[Mn(H_2O)_3)_2(H_2W_{12}O_{42})]_n^{6n-}$-type structures. MSF employed in this work have pore sizes between 2 and 3 nm, which makes particularly difficult the post-synthesis introduction of such linear structures. We therefore propose here to confine linear chains of $[Mn(H_2O)_3)_2(H_2W_{12}O_{42})]_n^{6n-}$ via their 'in situ' formation inside the nanoporous silica matrix using a soft sequential approach involving the immobilization of the $[Mn(H_2O)_6]^{2+}$ in a first step and their coordination to $[H_2W_{12}O_{42}]^{10-}$ units in a second step.

3.1. Electrochemical behaviour of $[(Mn(H_2O)_3)_2(H_2W_{12}O_{42})]_n^{6n-}$ in solution on bare ITO

Before proceeding with its immobilization, the electrochemical behavior of **1** has been studied by cyclic voltammetry (CV) on bare ITO electrode. Figure 1 shows typical CV curves recorded at various potential scan rates in aqueous medium (0.05 M Na_2SO_4 + H_2SO_4) at pH 3, in the potential window ranging from -0.5 to +1.4 V vs. Ag/AgCl. In the negative potentials window, one can see the first reversible signal corresponding to tungsten centers (*i.e.*, $W^{6+/5+}$ redox couple) in $[Mn(H_2O)_3)_2(H_2W_{12}O_{42})]_n^{6n-}$ but not subsequent reductions occurring at lower potential values (visible on carbon electrode [28] but not on ITO due to the limit in the potentials that can be reached on the cathodic side). When scanning potentials on the anodic side, one can see the electrochemical oxidation of Mn(II) centers of **1** (oxidation peak located at +1.05 V vs. Ag/AgCl) into Mn(IV) species, corresponding most likely to the formation of manganese oxide-based species (as reported for carbon electrode [28]). These manganese oxides partially redissolve on reverse scanning, which is characterized by the presence of a symmetrical cathodic peak located at +0.80 V vs. Ag/AgCl. The consecutive potential scans show a progressive shift of the anodic peak potential attributed to the continuous change in the nature of the surface due to the deposition of manganese oxides. When operating only towards negative potentials (Fig. 1B), the $W^{6+/5+}$ redox signal intensity is directly proportional to the square root of potential scan rates, indicating a diffusion-controlled process.

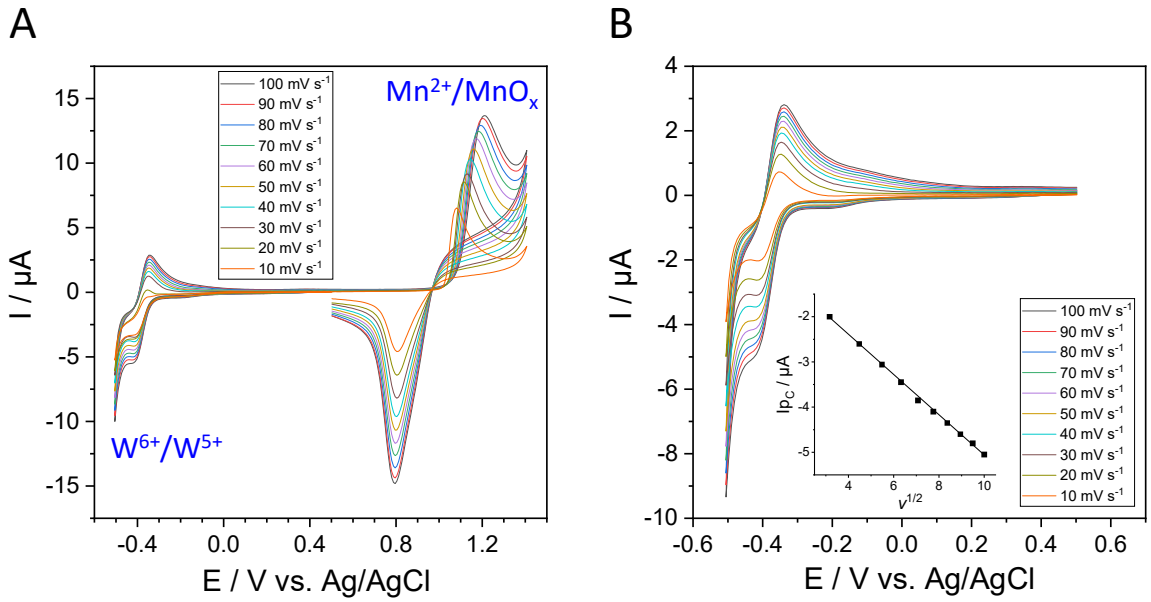

Figure 1. Cyclic voltammograms of $[Mn(H_2O)_3)_2(H_2W_{12}O_{42})]_n^{6n-}$ (**1**) recorded at various potential scan rates (from 100 to 10 mV s^{-1}) in an aqueous solution at pH 3 containing 0.5 mM of **1** (in 0.05 M Na_2SO_4 + H_2SO_4). (**A**) full potential window; (**B**) scanning potentials on the cathodic side only. Working electrode: ITO; temperature: 293° K.

3.2. 'In situ' formation of $[(Mn(H_2O)_3)_2(H_2W_{12}O_{42})]_n^{6n-}$ in vertically-oriented sulfonate-functionalized mesoporous silica thin films

1st step: Immobilization of $[Mn(H_2O)_6]^{2+}$ in the films.

The first step of the soft sequential process employed for the immobilization of the POM under mild experimental conditions (scheme 1) consists of the incorporation of $[Mn(H_2O)_6]^{2+}$ in the sulfonate-functionalized vertically-oriented silica films. It has been described previously that organosulfonate moieties can interact with transition-metal hexaaqua cations via hydrogen bonds, probably to stabilize the coordination complexes [33]. Within the H_2SO_4 concentration range considered in this work, Mn(II) will be found as the $[Mn(H_2O)_6]^{2+}$ hexaaqua ion in solution [34]. The sulfonate-functionalized silica films with various levels of functionalization

were dipped for 30 minutes in a solution containing 10 mM $MnCl_2 \cdot 4H_2O$. The successful immobilization of $[Mn(H_2O)_6]^{2+}$ inside the nanochannels was proved by cyclic voltammetry taking advantage of the electroactive nature of $[Mn(H_2O)_6]^{2+}$ cations at pH 3 (in 0.05 M Na_2SO_4 + H_2SO_4, see Figure 2). As shown, the voltammetric signals increased with sulfonate content (Fig. 2A), confirming the successful incorporation of larger amounts of manganese species into the films. On forward scan, one can observe an anodic wave with characteristic nucleation overpotentials, as commonly reported for metal electrodeposition [35]. This is especially visible at higher potential scan rates, and corresponds to the slow formation of manganese oxides [36], which are partially cathodically stripped on scan reversal, revealing a symmetrical cathodic peak located around 0.8-0.6 V depending on the potential scan rate (Fig. 2B). Finally, the evolution of the electrochemical response over 50 consecutive scans (as performed at 50 mV s^{-1}, see insert in Fig. 2A) indicated a decrease of the peak currents. This is most likely due to a progressive passivation of the surface by the deposited manganese oxides and/or to some leaching of Mn(II) species out of the film in the external solution.

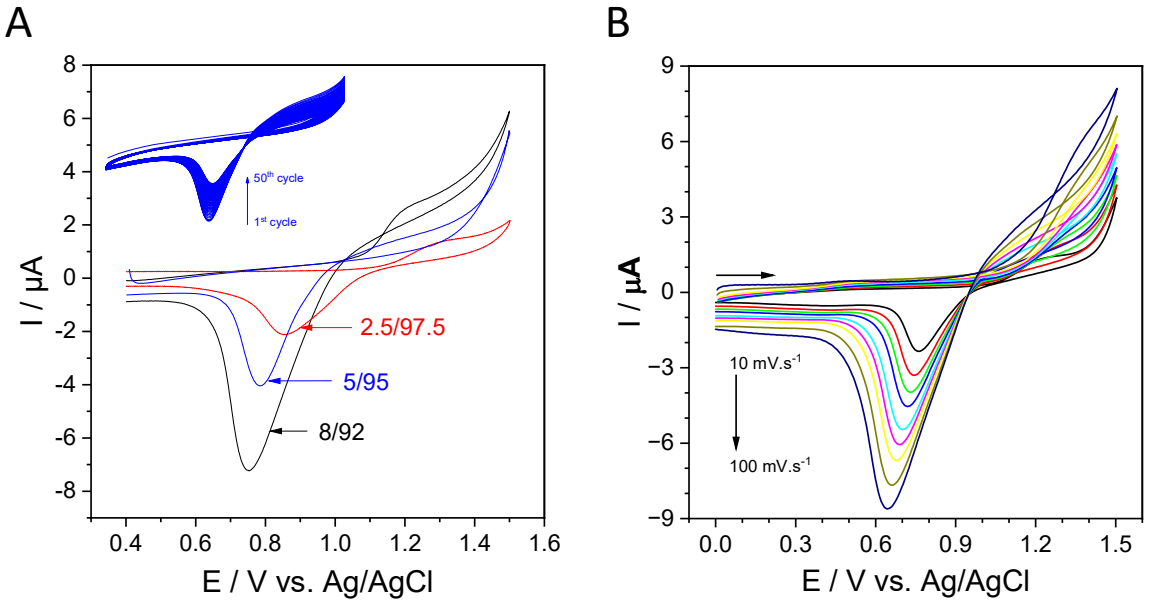

Figure 2. (**A**) CV curves of $[Mn(H_2O)_6]^{2+}SO_3^-@SiO_2$ films prepared on ITO electrode with CTAB and MPTMS/TEOS ratios of 2.5/97.5, 5/95 and 8/92, as recorded at a potential scan rate

of 50 mV s^{-1}; the insert shows 50 successive CV scans obtained with the 5/95 film. (**B**) CV curves of the 5/95 film, obtained at potential scan rates of 10, 20, 30, 40, 60, 70, 80, 90 and 100 mV s^{-1}. All the curves were recorded in aqueous 0.05 M Na_2SO_4 + H_2SO_4 (pH 3). Temperature: 293° K.

2nd step: 'In situ' formation of $[(Mn(H_2O)_3)_2H_2W_{12}O_{42}]_n^{6n-}$ in the nanochannels and influence of the initial composition of the film

Once the $[Mn(H_2O)_6]^{2+}$ are incorporated in the mesoporous matrix, the $[(Mn(H_2O)_3)_2(H_2W_{12}O_{42})]_n^{6n-}$ could be formed in the nanoporous channels by reaction with $Na_2WO_4 \cdot 2H_2O$, following a slightly modified procedure like that described for the preparation of the corresponding powder [28] (Scheme 1), adapted here to the pH constraints related to the chemical instability of the silica films in alkaline medium. An aqueous solution of $Na_2WO_4 \cdot 2H_2O$ is slowly added to a solution containing $Zn(CH_3COO)_2$ in acetate buffer (pH 4.6) buffer. Once the addition is complete and due to the basic nature of $Na_2WO_4 \cdot 2H_2O$, the pH of the solution increases up to 7.8 which is then reduced to 6 by addition of acetic acid in order to prevent any degradation of the silica membranes. The resulting solution is heated at 50°C for 15 min. After this period the previously prepared $[Mn(H_2O)_6]^{2+}SO_3^-@SiO_2$ materials functionalized at different degrees were dipped in this solution and heated at 65°C for a period of 1 hour in quiescent conditions to get the $[Mn_2W_{12}O_{42}]$POM-$SO_3^-@SiO_2$ films.

The proof of the formation of POM in the films is first given by cyclic voltammetry. Figure 3 compares the shape of the electrochemical response of the obtained functionalized films, showing an important evolution as a function of their initial sulfonate contents. For the films with a low content of sulfonate functions, *i.e.* MPTMS/TEOS 2.5/92.5 (see Fig. 3A) and 4/96 (not shown), the CV curves recorded in the studied potential window only show the presence

of manganese as electroactive species. This suggests that $[Mn(H_2O)_6]^{2+}$ cations are not sufficiently concentrated in the nanochannels to allow the formation of $[(Mn(H_2O)_3)_2(H_2W_{12}O_{42})]_n^{6n-}$ chains, but this does not necessarily mean the absence of monomeric tungsten species (that would not be electrochemically accessible in the potential window investigated here) such as $[H_2W_{12}O_{40})]^{6n-}$ or $[H_2W_{12}O_{42})]^{10n-}$ [28]. Indeed, EDX data (Table 1) indicates the presence of W in the silica film but largely in excess over Mn (*i.e.*, W/Mn ratio of about 12-13) compared to the ratio expected for the POM (6, corresponding to 12 W for 2 Mn). On the contrary, well-defined electrochemical response was obtained after 'in situ' formation of $[(Mn(H_2O)_3)_2(H_2W_{12}O_{42})]_n^{6n-}$ using mesoporous silica films prepared from MPTMS/TEOS ratios of 5/95 and 6.5/93.5 (see respectively parts B&C in Fig. 3). The curves exhibit the characteristic $W^{6+/5+}$ reversible peaks in the negative potential window and the typical Mn(II) oxidation signal on the anodic side, and the overall shapes observed are in good agreement to that obtained for **1** on bare ITO (Fig. 1) under the same experimental conditions (0.05 M Na_2SO_4 + H_2SO_4, pH 3). Again, this is consistent with EDX data indicating W/Mn molar ratios of 6-7 (Table 1), *i.e.* close to the value of 6 expected for $[(Mn(H_2O)_3)_2(H_2W_{12}O_{42})]_n^{6n-}$ chains.

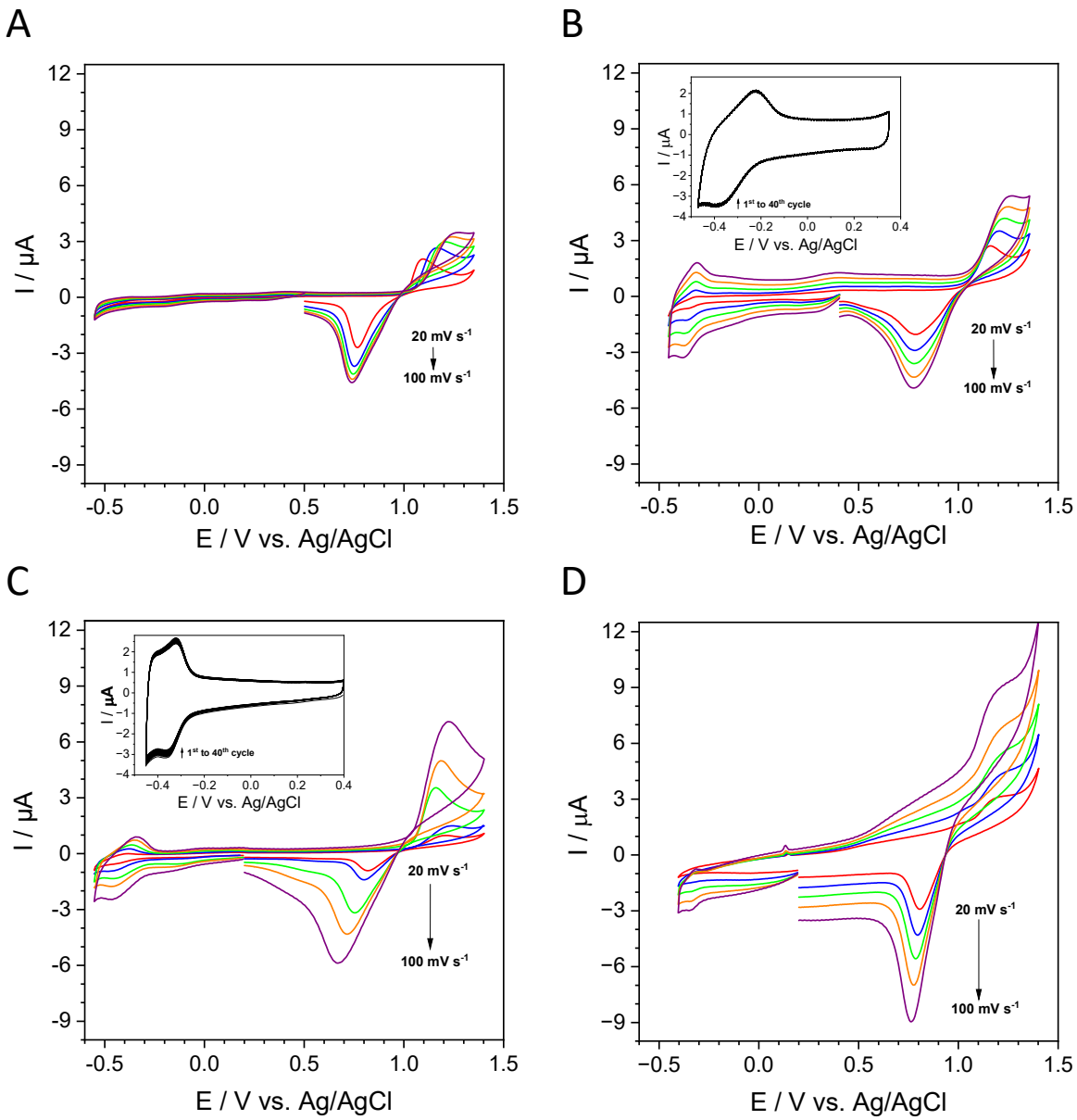

Figure 3. CV curves of $[Mn_2W_{12}O_{42}]$POM-SO_3^-@SiO_2 films prepared on ITO electrode with CTAB and MPTMS/TEOS ratios of (**A**) 2.5/97.5, (**B**) 5/95, (**C**) 6.5/93.5 and (**D**) 8/92, recorded in aqueous 0.05 M Na_2SO_4 + H_2SO_4 (pH 3) at potential scan rates of 20, 40, 60, 80 and 100 mV s^{-1}. The inserts in parts B and C show 40 successive CV scans obtained at 100 mV s^{-1} towards negative potential values corresponding to $W^{6+/5+}$ centers in the POM. Other conditions as in Fig. 2.

Table 1. TEM-EDX analyses of Mn and W at different points of the micrograph cross sections as a function of the functionalization level (MPTMS/TEOS ratio in the starting silica thin films).

MPTMS/TEOS ratio	At. Conc. % Mn	At. Conc. % W	W/Mn	Depth
2.5/97.5	1.0 ±0.1	12.6 ±0.8	12.6 ±1.5	15 nm
	1.1 ±0.1	12.5 ±0.8	11.4 ±1.3	45 nm
	1.0 ±0.1	12.8 ±0.8	12.8 ±1.5	65 nm
5/95	3.5 ±0.2	24.9 ±1.4	7.1 ±0.6	10 nm
	3.4 ±0.2	24.8 ±1.4	7.3 ±0.6	40 nm
	3.6 ±0.2	24.9 ±1.4	6.9 ±0.6	70 nm
6.5/93.5	4.2 ±0.2	25.5 ±1.4	6.1 ±0.5	20 nm
	4.1 ±0.2	25.6 ±1.4	6.2 ±0.5	50 nm
	4.1 ±0.2	25.5 ±1.4	6.2 ±0.5	80 nm
8/92	6.4 ±0.2	25.4 ±1.4	4.0 ±0.3	15 nm
	6.5 ±0.2	25.3 ±1.4	3.9 ±0.3	35 nm
	6.3 ±0.2	25.4 ±1.4	4.0 ±0.3	70 nm

Finally, the electrochemical behavior the film more concentrated in Mn^{2+} (prepared from 8/92 MPTMS/TEOS) made it possible to observe almost only the manganese signals in the positive potentials window, with only a residual small peak at -0.37 V (Fig. 3D). This suggests that the self-assembly of $[(Mn(H_2O)_3)_2(H_2W_{12}O_{42})]_n^{6n-}$ inside the nanochannels is hindered in this case, most likely due to the lack of space or unfavorable spatial distribution of such higher contents of sulfonate functions in the film. The W/Mn ratio of 4 observed for this 8/92 film (Table 1) also confirms the excess of unreacted manganese species. In conclusion, the observed electrochemical behavior highlights that the composition of the starting films, and in particular the content of sulfonate functions, plays an essential role in the successful synthesis of the $[(Mn(H_2O)_3)_2(H_2W_{12}O_{42})]_n^{6n-}$ inside the nanochannels of the silica matrix. So far, this 'in situ' synthesis is the only way to immobilize such POM in oriented mesoporous silica films since 'simple' impregnation with $[(Mn(H_2O)_3)_2(H_2W_{12}O_{42})]^{6n-}$ species did not allow their effective incorporation inside the nanochannels due to electrostatic repulsions induced by the negatively-charged silica walls (which is known to reject anions [7]).

3.3. Further characterization of $[Mn_2W_{12}O_{42}]$POM-SO_3^-@SiO_2 films and effect of pore size

Figure 4 displays typical TEM imaging (top view and cross-section) of $[Mn_2W_{12}O_{42}]$POM-SO_3^-@SiO_2 films, where one can clearly see that the degree of order and hexagonal packing of the mesopore channels are maintained after generation of the $[(Mn(H_2O)_3)_2(H_2W_{12}O_{42})]_n^{6n-}$ chains inside the mesoporous film (Fig. 4A) and that all nanochannels are vertically oriented (Fig. 4B). This is consistent with previous observations on functionalized mesoporous silica membranes prepared by EASA [8, 37], but it also indicates that the conditions applied here for POM synthesis are compatible with the chemical stability of the silica matrix. EDX analysis (Fig. 4C) at different depth of TEM cross-section micrographs (as summarized in Table 1) show a homogeneous distribution of the different elements indicating a uniform composition through the whole length of the mesopores. The GISAXS pattern (Fig. 4D) confirms that the regular and vertically oriented hexagonal structure is maintained over the whole film area, with a characteristic diffraction spot at 1.7 nm^{-1} [8]. When confined in the nanochannels, the POM chains are characterized by good operational stability, as evidenced by the almost identical CV curves recorded under multi-scan conditions (see inserts in Fig. 3B&C). After 40 potential scans at 100 mV s^{-1}, a decrease of the signal by only 4% was observed for the 5/95 film and 12% for the 6.5/93.5 film. For the 'best' film (*i.e.*, as prepared from 5/95 MPTMS/TEOS ratio), integrating the area under the cathodic peak gave a value of 4.5 μC, which would correspond (taking into account the Faraday law and one electron exchanged per POM) to 27 10^{12} POM units that are electrochemically accessible. Considering a mesopore density of 5 10^{12} pores per cm^2 (as assessed from TEM, Fig. 5A) and an electrode surface area of 0.20 cm^2, this would roughly correspond to 27 POM per nanochannel involved in the electrochemical processes. Although no thermal stability experiments have been performed here, it is expected to be good as tungsten-based POMs are often stable up to 500°C or higher and silica is also highly thermally stable, keeping its structural and chemical integrity at temperature above 1000°C.

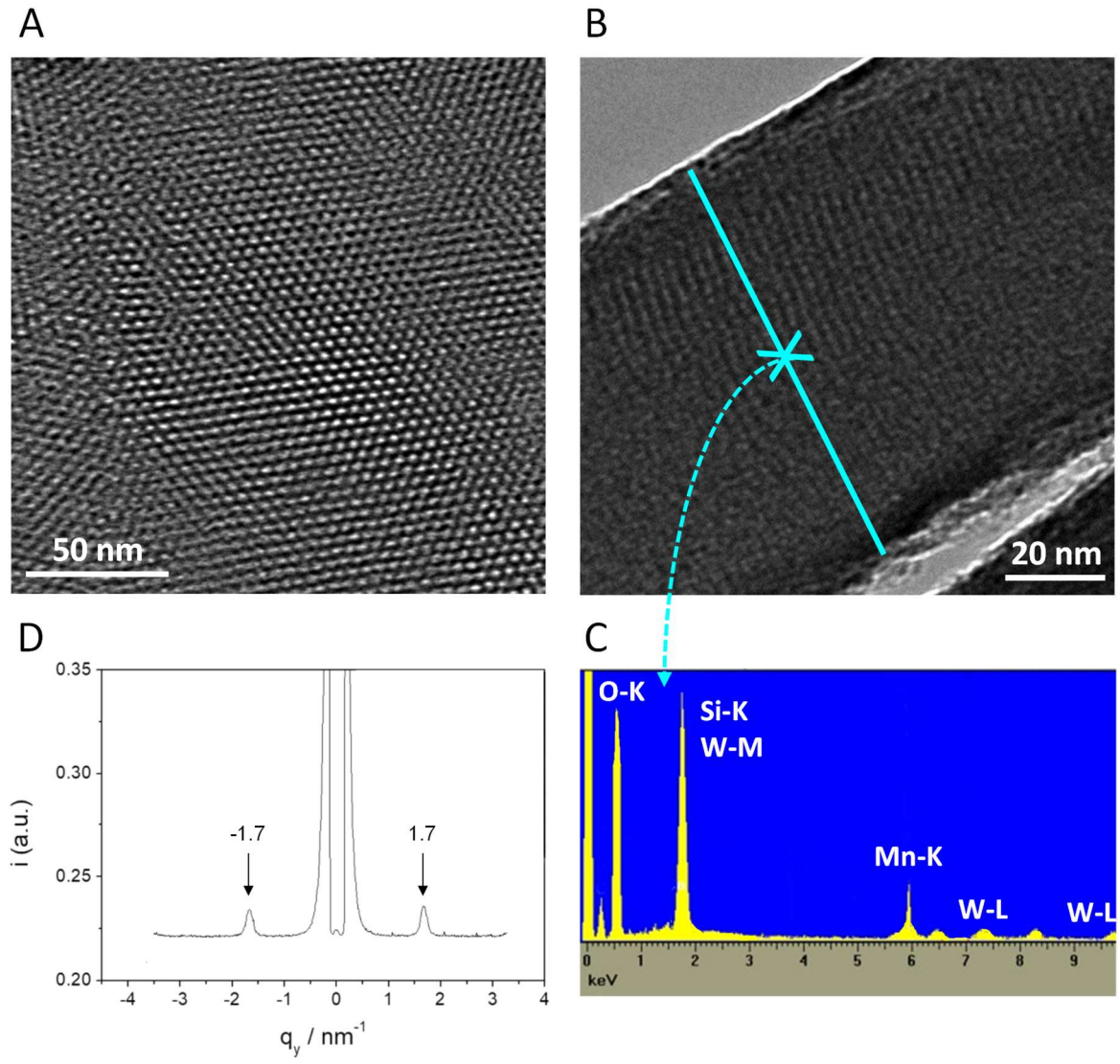

Figure 4. TEM (**A**) top view and (**B**) cross-section of $[Mn_2W_{12}O_{42}]$POM-SO_3^-@SiO_2 films prepared with MPTMS/TEOS ratio of 5/95 using CTAB surfactant. (**C**) corresponding EDX spectra recorded on the cross-section (at blue arrow). (**D**) GISAXS intensity profile plotted against q_y.

As illustrated in Figure 5 for the 5/95 film, the presence of POM was also evidenced by XPS by comparing the signals of Mn2p and W4f core levels respectively obtained before and after formation of the POM. The $[Mn(H_2O)_6]^{2+}SO_3^-$@SiO_2 film exhibited the characteristic $Mn2p_{3/2}$

and $Mn2p_{1/2}$ peaks (respectively located at 641.8 eV and 653.6 eV, with a small satellite signal at 645 eV (Fig. 5A), consistent with binding energies and spin-orbit splitting reported for Mn(II) species [38, 39], and obviously no signal for W (Fig. 5B). The Mn atomic percent contents increased with the sulfonate functionalization levels, confirming larger amounts of Mn^{2+} ions in the $[Mn(H_2O)_6]^{2+}SO_3^-@SiO_2$ films (consistent with CV data, Fig. 1), but also S/Mn ratios around 3 or slightly larger (Table 2) indicating that not all sulfonate groups are involved in the binding of $[Mn(H_2O)_6]^{2+}$ as a result of unfavorable distribution on the mesopore walls (some of them remained "free") as previously observed for $Fe^{2+}SO_3^-@SiO_2$ films [29]. On the contrary, well-defined W4f signals ($W4f_{7/2}$ and $W4f_{5/2}$ peaks centered respectively at 36.2 eV and 38.4 eV) characteristic of $[Mn(H_2O)_3)_2(H_2W_{12}O_{42})]_n^{6n-}$ species [28], were obtained for the $[Mn_2W_{12}O_{42}]$POM-$SO_3^-@SiO_2$ films (Fig. 5D). Also, $Mn2p_{3/2}$ and $Mn2p_{1/2}$ signals of the $[Mn_2W_{12}O_{42}]$POM-$SO_3^-@SiO_2$ film (Fig. 5C) were broader than those of the $[Mn(H_2O)_6]^{2+}SO_3^-@SiO_2$ film and centered at slightly different binding energies (respectively 641.4 eV and 654.1 eV, see Fig. 5A) but consistent with data reported for other Mn-based POMs [40, 41], suggesting a different chemical environment for Mn(II) species in the POM compared to the "free" $[Mn(H_2O)_6]^{2+}$ species. In agreement with the EDX data above (Table 1), the observed W/Mn atomic ratios were close to the value of 6 expected for the POM with 5/95 and 6.5/93.5 films but deviated ideality for the others (Table 2) for the same reasons as above, confirming the successful formation of the POM at a functionalization level around 5-6.5% of sulfonate groups in the material. Overall, although XPS revealed only surface concentrations, EDX reported total Mn and W contents throughout the film thickness, and electrochemistry provided information only on electrochemically accessible POM species, all results demonstrated the critical effect of the amount of sulfonate groups in the starting material to achieve efficient formation of the target $[Mn(H_2O)_3)_2(H_2W_{12}O_{42})]_n^{6n-}$ POM in the mesoporous films in an electroactive and stable form.

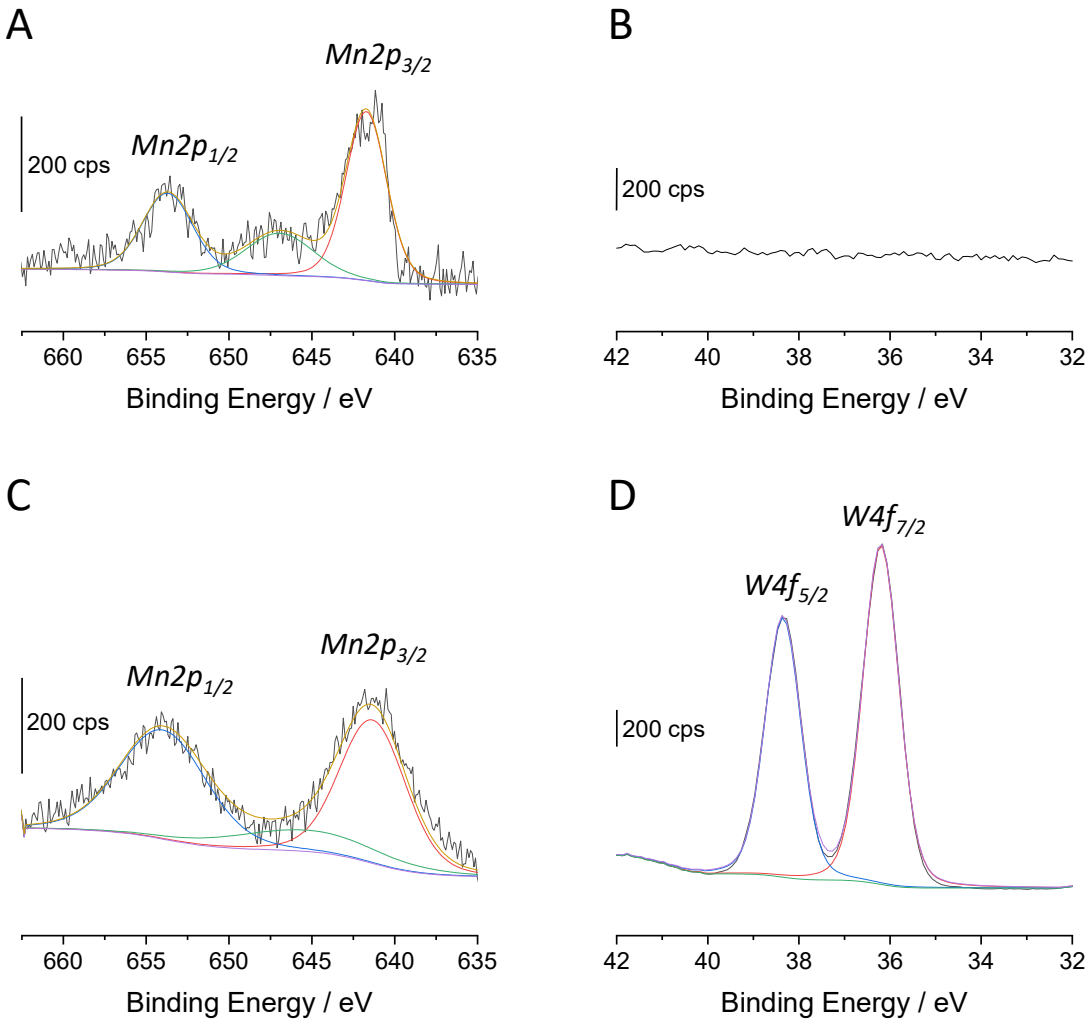

Figure 5. (**A**, **C**) Mn2p and (**B**, **D**) W4f core level spectra recorded for (**A**, **B**) $[Mn(H_2O)_6]^{2+}SO_3^-$@SiO_2 and (**C**, **D**) $[Mn_2W_{12}O_{42}]$POM-SO_3^-@SiO_2 films prepared from 5/95 MPTMS/TEOS ratio.

Table 2. Sulfur, manganese, and tungsten, relative atomic surface concentration (%At.) obtained from XPS data for $[Mn(H_2O)_6]^{2+}SO_3^-@SiO_2$ and $[Mn_2W_{12}O_{42}]$POM-$SO_3^-@SiO_2$ films prepared from various MPTMS/TEOS ratios.

$[Mn(H_2O)_6]^{2+}SO_3^-@SiO_2$			
MPTMS/TEOS ratio	At. Conc. % S	At. Conc. % Mn	S/Mn
2.5/97.5	2.3	0.8	3.1
5/95	5.2	1.6	3.2
6.5/93.5	6.3	1.8	3.5
8/92	7.4	2.4	3.1
$[Mn_2W_{12}O_{42}]$POM-$SO_3^-@SiO_2$			
MPTMS/TEOS ratio	At. Conc. % Mn	At. Conc. % W	W/Mn
2.5/97.5	1.8	17.3	9.6
5/95	4.1	25.2	6.2
6.5/93.5	4.9	28.1	5.7
8/92	6.5	18.3	2.8

Finally, experiments similar to those above were performed with mesoporous silica films having a larger pore diameter (*i.e.*, 3 nm instead of 2 nm, as prepared from ODAB instead of CTAB surfactant [42]) and showing a similar hexagonal structure pore orientation and composition as determined from TEM-EDX measurements (data not shown). Their behaviour was very similar those described above. Figure 6 displays typical CV curves obtained for $[Mn_2W_{12}O_{42}]$POM-$SO_3^-@SiO_2$ films prepared from MPTMS/TEOS ratios of 5/95 (Fig. 6A) and 6.5/93.5 (Fig. 6B). As shown, they exhibit the characteristic $W^{6+/5+}$ reversible peaks on the cathodic side and the Mn(II) oxidation signal when going to the anodic direction. The tungsten signals coming from the species $[Mn(H_2O)_3)_2(H_2W_{12}O_{42})]_n^{6n-}$ are of fairly similar intensities, indicating that similar amounts of $[Mn(H_2O)_6]^{2+}$ cations are necessary in these larger nanochannels to enable successful formation of POM by reaction with $Na_2WO_4{\bullet}2H_2O$ (pore

size does not seem to have any significant effect on the 'in situ' POM formation). Even if the POM is immobilized into the film casted onto the electrode surface, its voltammetric behavior exhibits a characteristic diffusive component originating from the restricted transport of counterions from the solution to maintain charge balance in the film, as common for this kind of films functionalized with redox-active chains [8]. Again, when successfully generated in the mesoporous film, the $[Mn(H_2O)_3)_2(H_2W_{12}O_{42})]_n^{6n-}$ chains exhibited quite good operational stability as evidenced by multisweep CV, yet with some more decrease in cathodic currents (*i.e.*, -17% after 25 cycles, see inserts in Fig. 6) which could be due to low leaching from these larger nanochannels.

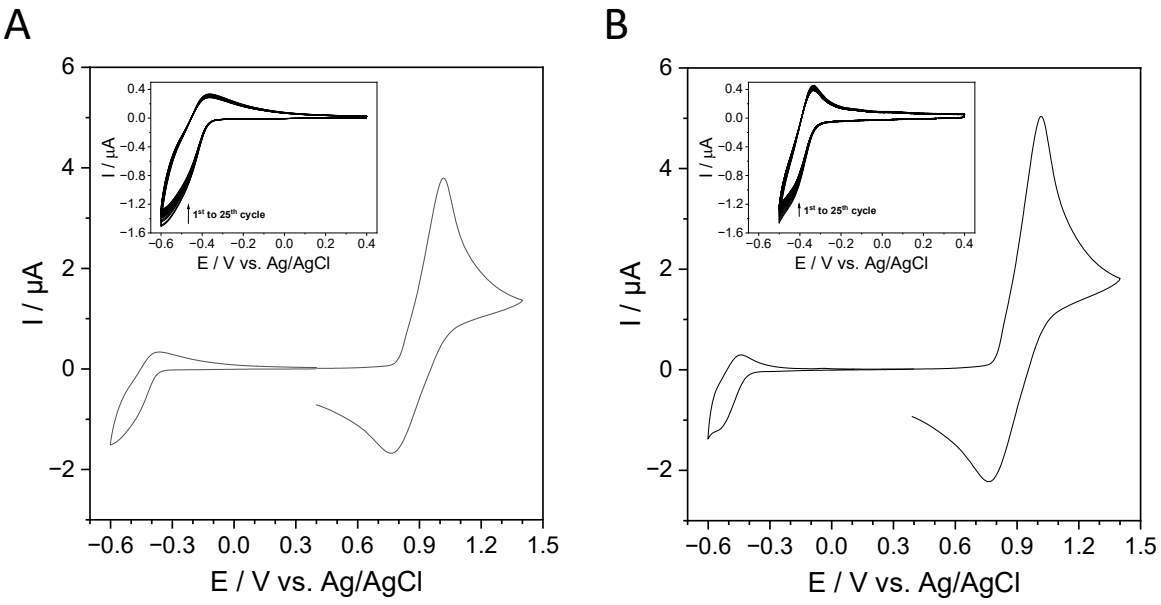

Figure 6. CV curves of $[Mn_2W_{12}O_{42}]$POM-SO_3^-@SiO_2 films prepared on ITO electrode with ODAB and MPTMS/TEOS ratios of (**A**) 5/95 and (**B**) 6.5/93.5, recorded in aqueous 0.05 M Na_2SO_4 + H_2SO_4 (pH 3) at a potential scan rate of 100 mV s^{-1}. The insert in part B shows 25 successive CV scans sampled to more negative potentials corresponding to $W^{6+/5+}$ redox couple. Other conditions as in Fig. 2.

4. Conclusions

This work demonstrates the successful 'in situ' synthesis of $[(Mn(H_2O)_3)_2(H_2W_{12}O_{42}]^{6n-}$ POM species inside vertically aligned mesoporous silica thin films of 2 and 3 nm pore sizes on ITO electrodes. This is possible thanks to the confinement of $[Mn(H_2O)_6]^{2+}$ in sulfonate-functionalized silica films and their subsequent reaction with $Na_2WO_4 \bullet 2H_2O$ provided that there is an adequate sulfonate content in the material (5-6.5 %). When immobilized, this POM remains electrochemically accessible in spite of the insulating properties of the silica matrix. So far, such POM structures can be only obtained in a durably immobilized form on an electrode surface according to this 'in situ' formation strategy, also applicable to other POMs [43] or to metal polypyridyl complexes [44] and offering stable operational stability during multi-scan cyclic voltammetry.

Acknowledgements

The authors thank the funding from ANR POMSIL (Project ANR-20-CE09-0004 of the French *Agence Nationale de la Recherche*). They are also grateful to Jaafar Ghanbaja from the *Institut Jean Lamour* for TEM-EDX measurements.

References

[1] A. Corma, From microporous to mesoporous molecular sieve materials and their use in catalysis, Chem. Rev. 97 (1997) 2373–2419. https//doi.org/10.1021/cr960406n.

[2] G. Ferey, G. Hybrid porous solids: past, present, future, Chem. Soc. Rev. 37 (2008) 191–214. https//doi.org/10.1039/B618320B

[3] Y. Wan, D. Zhao, On the controllable soft-templating approach to mesoporous silicates, Chem. Rev. 107 (2007) 2821–2860. https//doi.org/10.1021/cr068020s.

[4] A. Walcarius, E. Sibottier, M. Etienne, J. Ghanbaja, Electrochemically-assisted self-assembly of mesoporous silica thin films, Nat. Mater. 6 (2007), 602–608. https//doi.org/10.1038/nmat1951.

[5] Z. Teng, G. Zheng, Y. Dou, W. Li, C.-Y. Mou, X. Zhang, A. M. Asiri, D. Zhao, Highly ordered mesoporous silica films with perpendicular mesochannels by a simple Stöber-solution growth approach, Angew. Chem. Int. Ed. 51 (2012) 2173–2177. https://doi.org/10.1002/anie.201108748.

[6] P. Zhou, L. Yao, K. Chen, B. Su, Silica nanochannel membranes for electrochemical analysis and molecular sieving: A comprehensive review, Crit. Rev. Anal. Chem. 50 (2020) 424–444. https://doi.org/10.1080/10408347.2019.1642735.

[7] A. Walcarius, Electroinduced surfactant self-assembly driven to vertical growth of oriented mesoporous films, Acc. Chem. Res. 54 (2021) 3563–3575. https://doi.org/10.1021/acs.accounts.1c00233.

[8] W. Ullah, G. Herzog, N. Vilà, A. Walcarius, Polyaniline nanowire arrays generated through oriented mesoporous silica films: effect of pore size and

spectroelectrochemical response, Faraday Discuss. 233 (2022) 77–99. https://doi.org/10.1039/D1FD00034A.

[9] A. M. R. Ramírez, M. A. del Valle, E. Ortega, F. R. Díaz, M. A. Gacitúa, Capacitors based on polypyrrole nanowire electrodeposits, Polymers 14 (2022) 5476. https://doi.org/10.3390/polym14245476.

[10] Y. Liang, Recent advanced development of metal-loaded mesoporous organosilicas as catalytic nanoreactors, Nanoscale Adv. 3 (2021) 6827. https://doi.org/10.1039/d1na00488c.

[11] M. L. Scala-Benuzzi, S. N.Fernández, G. Giménez, G. Ybarra, G. J. A. A. Soler-Illia, Ordered mesoporous electrodes for sensing applications, ACS Omega 8 (2023) 24128−24152. https://doi.org/10.1021/acsomega.3c02013.

[12] M. T. Pope, A. Müller, Polyoxometalate chemistry: an old field with new dimensions in several disciplines, Angew. Chem. Int. Ed. 30 (1991) 34–48. https//doi.org/10.1002/anie.199100341.

[13] M. Sadakane, E. Steckhan, Electrochemical properties of polyoxometalates as electrocatalysts, Chem. Rev. 98 (1998) 219–237. https://doi.org/10.1021/cr960403a.

[14] D. L. Long, R. Tsunashima, L. Cronin, Polyoxometalates: building blocks for functional nanoscale systems, Angew. Chem. Int. Ed. 49 (2010) 1736–1758. https://doi.org/10.1002/anie.200902483.

[15] T. Ueda, Electrochemistry of polyoxometalates: from fundamental aspects to applications, ChemElectroChem 5 (2018) 823–838. https://doi.org/10.1002/celc.201701170.

[16] C. Freire, D. M. Fernandes, M. Nunes, M. Araújo, Polyoxometalate-based modified

electrodes for electrocatalysis: from molecule sensing to renewable energy-related applications, in: Advanced Electrode Materials, Eds. A. Tiwari, F. Kuralay, L. Uzun, Scrivener Publishing LLC, Beverly, Massachusetts, 2016, Chap. 5, pp. 147–212. https://doi.org/10.1002/9781119242659.ch5.

[17] M. Ammam, Polyoxometalates: formation, structures, principal properties, main deposition methods and application in sensing, J. Mater. Chem. A 1 (2013) 6291–6312. https://doi.org/10.1039/c3ta01663c.

[18] L. Zhang, Z. Chen, Polyoxometalates: tailoring metal oxides in molecular dimension toward energy applications, Int. J. Energ. Res. 44 (2020) 3316–3346. https://doi.org/10.1002/er.5124.

[19] S. M. Wang, J. Hwang, E. Kim, Polyoxometalates as promising materials for electrochromic devices, J. Mater. Chem. C 7 (2019) 7828–7850. https://doi.org/10.1039/c9tc01722d.

[20] T. McCormac, D. Farrell, D. Drennan, G. Bidan, Immobilization of a series of Dawson type heteropolyanions, Electroanalysis 13 (2001) 836–842. https://doi.org/10.1002/1521-4109(200106)13:10<836::AID-ELAN836>3.0.CO;2-F.

[21] B. Wang, L. Cheng, S. Dong, Construction of a heteropolyanion-modified electrode by a two-step sol-gel method and its electrocatalytic applications, J. Electroanal. Chem. 516 (2001) 17–22. https://doi.org/10.1016/S0022-0728(01)00677-5.

[22] P. J. Kulesza, K. Karnicka, K. Miecznikowski, M. Chojak, A. Kolary, P. J. Barczuk, G. Tsirlina, W. Czerwinski, Network electrocatalytic films of conducting polymer-linked polyoxometalate-stabilized platinum nanoparticles, Electrochim. Acta 5 (2005) 5155–5162. https://doi.org/10.1016/j.electacta.2005.03.061.

[23] M. Genovese, Y. W. Foong, K. Lian, Designing polyoxometalate based layer-by-layer

thin films on carbon nanomaterials for pseudocapacitive electrodes, J. Electrochem. Soc. 162 (2015) A5041–A5046. https://doi.org/10.1149/2.0071505jes.

[24] L. Vilà-Nadal, S. G. Mitchell, S. Markov, C. Busche, V. Georgiev, A. Asenov, L. Cronin, Towards polyoxometalate-cluster-based nano-electronics, Chem. Eur. J. 19 (2013) 16502–16511. https://doi.org/10.1002/chem.201301631.

[25] A. Dolbecq, E. Dumas, C. R. Mayer, P. Mialane, Hybrid organic-inorganic polyoxometalate compounds: From structural diversity to applications. Chem. Rev. 110 (2010) 6009–6048. https://doi.org/10.1021/cr1000578.

[26] S. Liu, Z. Tang, Polyoxometalate-based functional nanostructured films: Current progress and future prospects, Nano Today 5 (2010) 267–281. https://doi.org/10.1016/j.nantod.2010.05.006.

[27] R. Zhang, C. Yang, A novel polyoxometalate-functionalized mesoporous hybrid silica: synthesis and characterization, J. Mater. Chem. 18 (2008) 2691–2703. https://doi.org/10.1039/b800025e.

[28] A. L. Teillout, P. de Oliveira, J. Marrot, R. C. Howell, N. Vilà, A. Walcarius, I. M. Mbomekallé, Synthesis, crystal structure, electrochemistry and electro-catalytic properties of manganese-containig polyoxotungstate, $[(Mn(H_2O)_3)_2(H_2W_{12}O_{42})]^{6-}$, Inorganics 7 (2019) 15. https://doi.org/10.3390/inorganics7020015.

[29] S. Ahoulou, C. Richart, C. Carteret, S. Pillet, N. Vilà, A. Walcarius, Weak coordinating character of organosulfonates in oriented silica films: an efficient approach for immobilizing cationic meta-transition complexes, Molecules 17 (2022), 5444. https://doi.org/10.3390/molecules27175444.

[30] G. Herzog, E. Sibottier, M. Etienne, A. Walcarius, Electrochemically-assisted self-assembly of ordered and functionalized mesoporous silica films: impact of the

electrode geometry and size on film formation and properties, Faraday Discuss. 164 (2013) 259–273. https://doi.org/10.1039/C3FD00021D.

[31] N. Vilà, A. Walcarius, Electrochemical response of vertically-aligned, ferrocene-functionalized mesoporous silica films: effect of supporting electrolyte, Electrochim. Acta 179 (2015) 304–314. https://doi.org/10.1016/j.electacta.2015.02.169.

[32] A. Goux, M. Etienne, E. Aubert, C. Lecomte, J. Ghanbaja, A. Walcarius, Oriented mesoporous silica films obtained by electro-assisted self-assembly (EASA), Chem. Mater. 21 (2009) 731–741. https://doi.org/10.1021/cm8029664.

[33] R. Singh, G. Kociok-Köhn, K. Singh, S. Kumar Pandey, L. Singh, Influence of ligand coordination: solvent and non-covalent interaction on the structural outcomes in coordination polymers with direct Cd(II)-alkanesulfonate bonds: a combined experimental and computational study, J. Sol. State Chem. 280 (2019) 120992. https://doi.org/10.1016/j.jssc.2019.120992.

[34] C. J. Clarke, G. J. Browning, S. W. Donne, An RDE and RRDE study into the electrodeposition of manganese dioxide, Electrochim. Acta 51 (2006) 5773–5784. https://doi.org/10.1016/j.electacta.2006.03.013.

[35] I. Danaee, F. Shoghi, M. Dehghani Mobarake, M. Kameli, Electrocrystallization of palladium from $Pd(NH_3)_4Cl_2$ bath on stainless steel 316L, J Solid State Electrochem. 14 (2010) 57–62. https://doi.org/10.1007/s10008-009-0788-3.

[36] S. Thiagarajan, T. H. Tsai, S.-M. Chen, Electrochemical fabrication of nano manganese oxide modified electrode for the detection of H_2O_2, Int. J. Electrochem. Sci. 6 (2011) 2235–2245. https://doi.org/10.1016/s1452-3981(23)18180-6.

[37] N. Vilà, A. Walcarius, Electrochemically assisted generation of highly ordered azide-functionalized mesoporous silica for oriented hybrid films, Angew. Chem. Int. Ed. 17

(2014), 2945–2950. https://doi.org/10.1002/anie.201309447.

[38] B. J. Tan, K. J. Klabunde, P. A. Sherwood, XPS studies of solvated metal atom dispersed catalysts. Evidence for layered cobalt-manganese particles on alumina and silica, J. Am. Chem. Soc. 113 (1991) 855–861. https://doi.org/10.1021/ja00003a019.

[39] P. Xiong, G. Zeng, L. Zenga, M. Wei, Prussian blue analogues $Mn[Fe(CN)_6]_{0.6667}\cdot nH_2O$ cubes as an anode material for lithium-ion batteries, Dalton Trans. 44 (2015) 16746–16751. https://doi.org/10.1039/c5dt03030g.

[40] X. Xing, M. Wang, R. Liu, S. Zhang, K. Zhang, B. Li, G. Zhang, Highly efficient electrochemically driven water oxidation by graphene-supported mixed-valent Mn 16-containing polyoxometalate, Green Energy Environ. 1 (2016) 138e143. https://doi.org/10.1016/j.gee.2016.04.001.

[41] W. Li, P. Luo, Z. Fu, X. Yuan, M. Huang, K. Wan, Z. Xiang, Z. Liang, Highly reversible and stable manganese(II/III)-centered polyoxometalates for neutral aqueous redox flow battery, Next Energy 1 (2023) 100028. https://doi.org/10.1016/j.nxener.2023.100028.

[42] N. Vilà, E. André, R. Ciganda, J. Ruiz, D. Astruc, A. Walcarius, Molecular sieving with vertically-aligned mesoporous silica films and electronic wiring through isolating nanochannels, Chem. Mater. 28 (2016) 2511–2514. https://doi.org/10.1021/acs.chemmater.6b00716.

[43] N. Vilà, L. Nguyen, J.-C. Lacroix, X. Sun, A. Walcarius, I. M. Mbomekallé, Assessing the influence of confinement on the stability of $[MP_2W_{17}O_{61}]^{7-}$-functionalized surfaces: A soft sequential immobilization approach for electrochromic devices, *ACS Appl. Mater. Interfaces*, 16 (2024), 26521–26536. https://doi.org/10.1021/acsami.4c01859.

[44] N. Vilà, A. Walcarius, Bis(terpyridine) Iron(II) functionalized vertically-oriented

nanostructured silica films: towards electrochromic materials, Front. Chem. 8 (2020) 830. https://doi.org/10.3389/fchem.2020.00830.